Electronic Supplementary Information

Tricomponent Brookite/Anatase TiO_2/g-C_3N_4 Heterojunction in Mesoporous Hollow Microspheres for Enhanced Visible-light Photocatalysis

Hao Wei, William A. McMaster, Jeannie Z. Y. Tan, Dehong Chen* and Rachel A. Caruso*
Rachel.Caruso@rmit.edu.au

Fig. S1 Optical photos of a) MBA, b) MBACN-1, c) MBACN-2, d) MBACN-3, and e) CN.

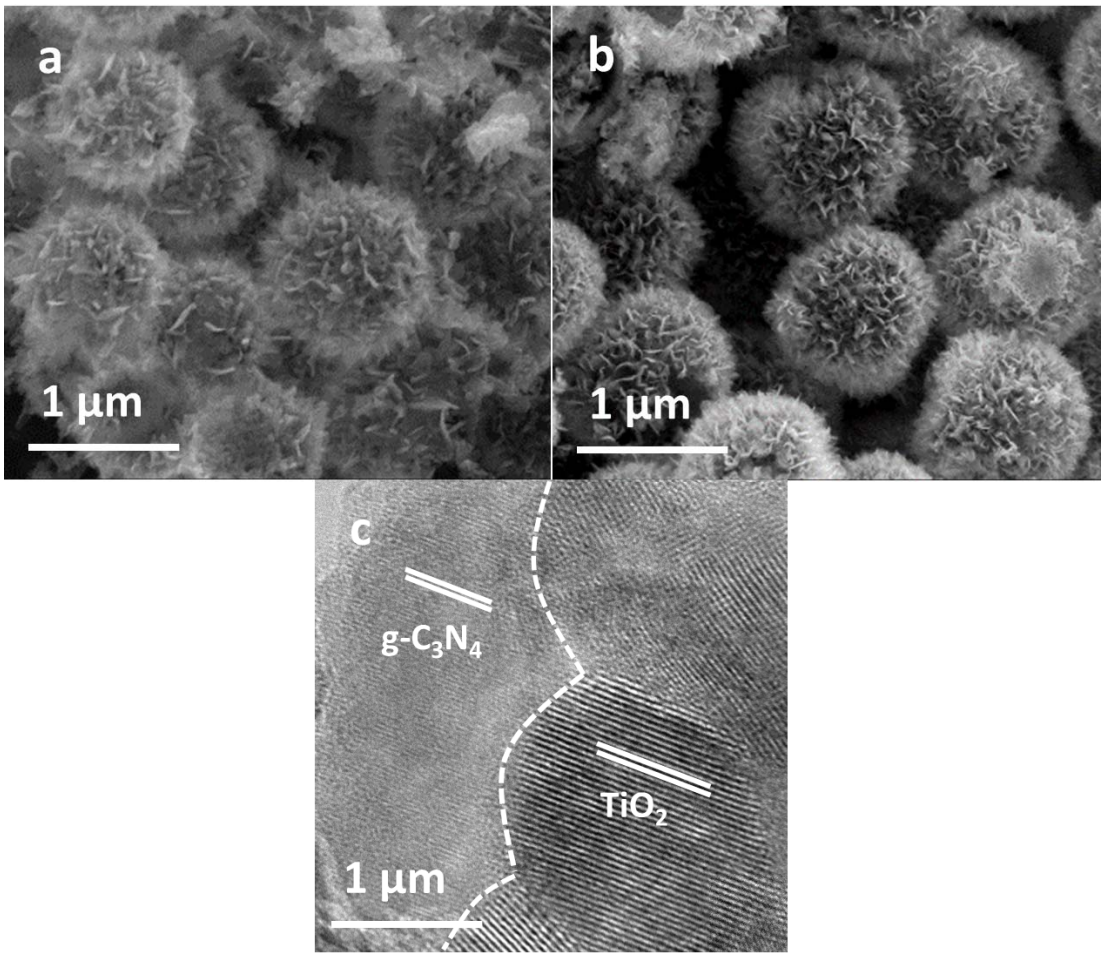

Fig. S2 SEM images of a) MBACN-1 and b) MBACN-3. c) HRTEM image of MBACN-2.

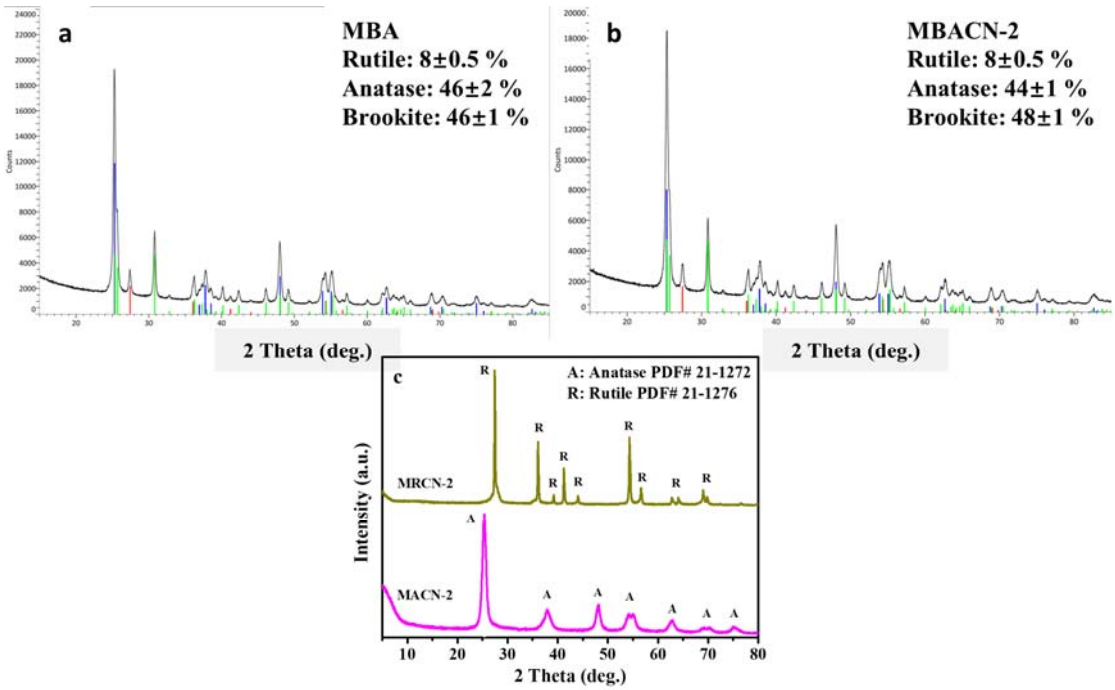

Fig. S3 Rietveld refinement of a) MBA and b) MBACN-2. c) XRD patterns of MACN-2 and MRCN-2.

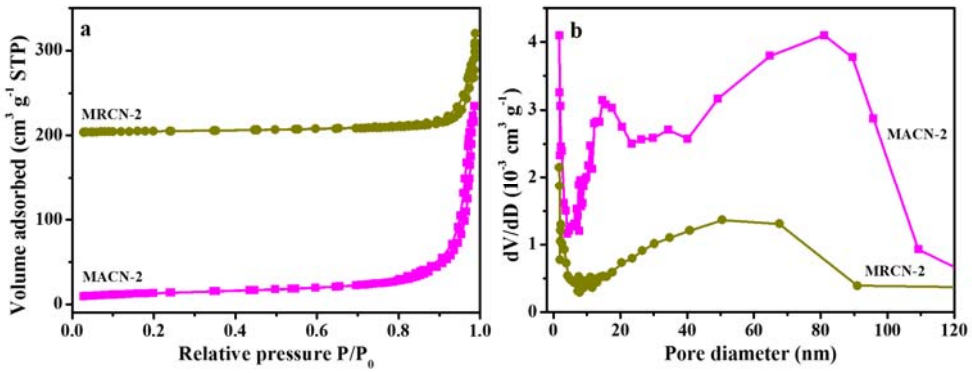

Fig. S4 a) Nitrogen sorption isotherms and b) BJH pore size distributions of MACN-2 and MRCN-2. The isotherm of MRCN-2 is offset vertically by 200 cm^3 g^{-1}.

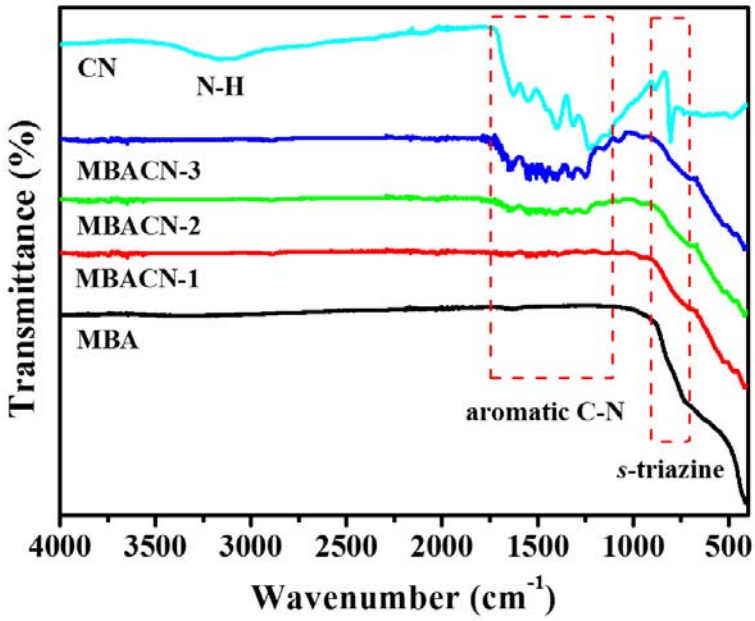

Fig. S5 FT-IR spectra of MBA, MBACN-*x*, and CN.

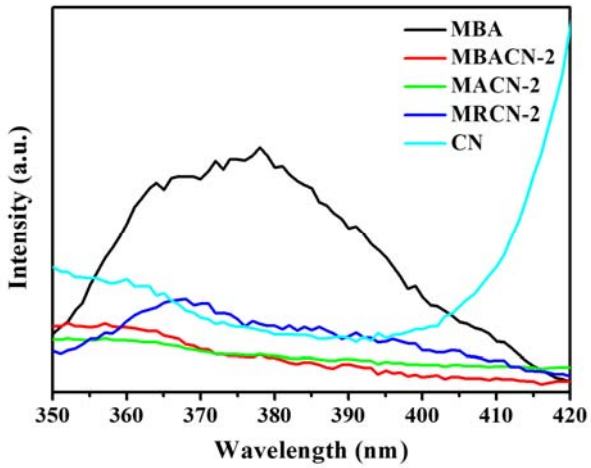

Fig. S6 Enlarged PL spectra for MBA, MBACN-2, MACN-2, MRCN-2, and CN in the range 350 nm to 420 nm.

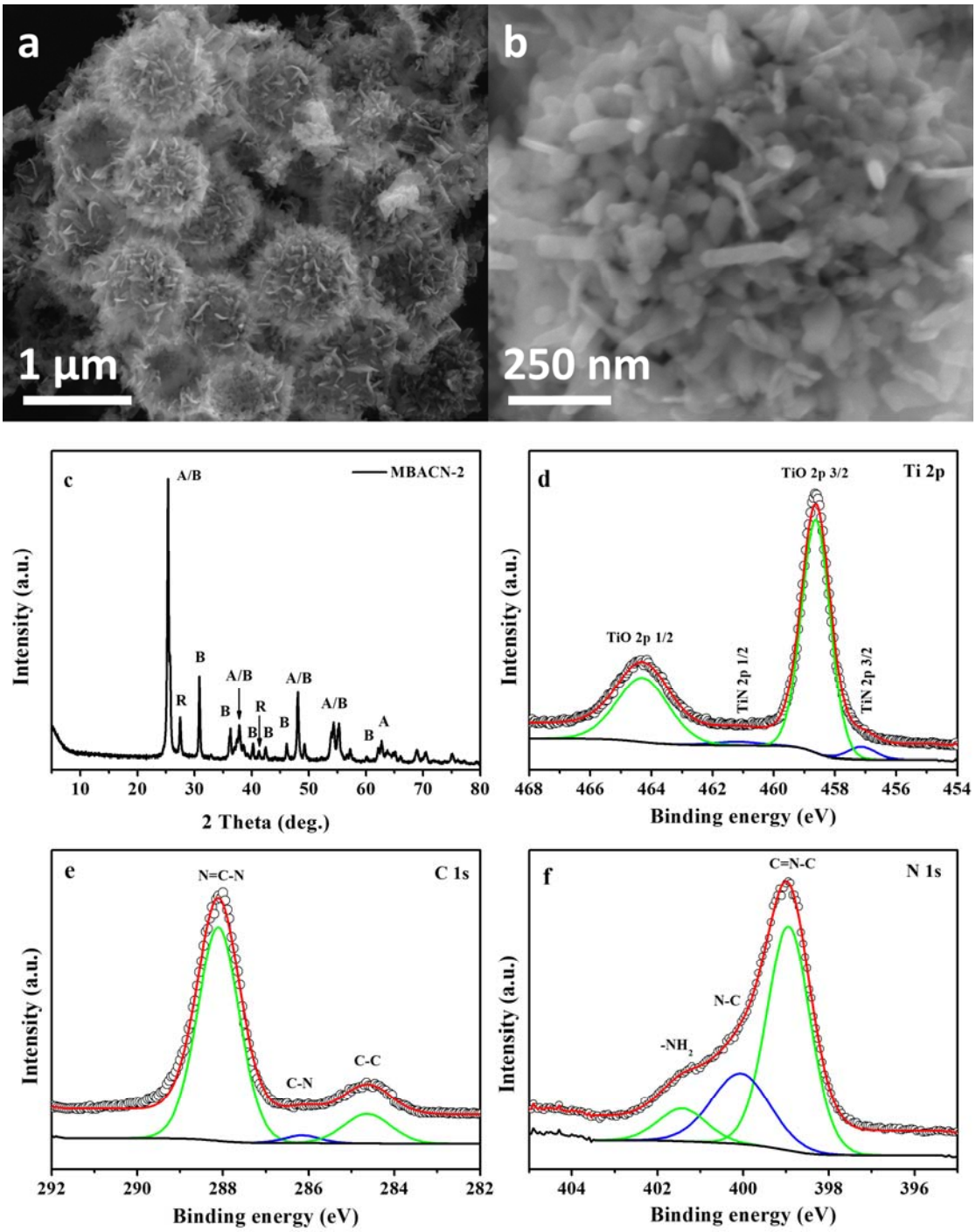

Fig. S7 a) and b) SEM images, c) XRD pattern, d) Ti 2p, e) C 1s and f) N 1s XPS of MBACN-2 after 5 cycles of photocatalytic reaction.

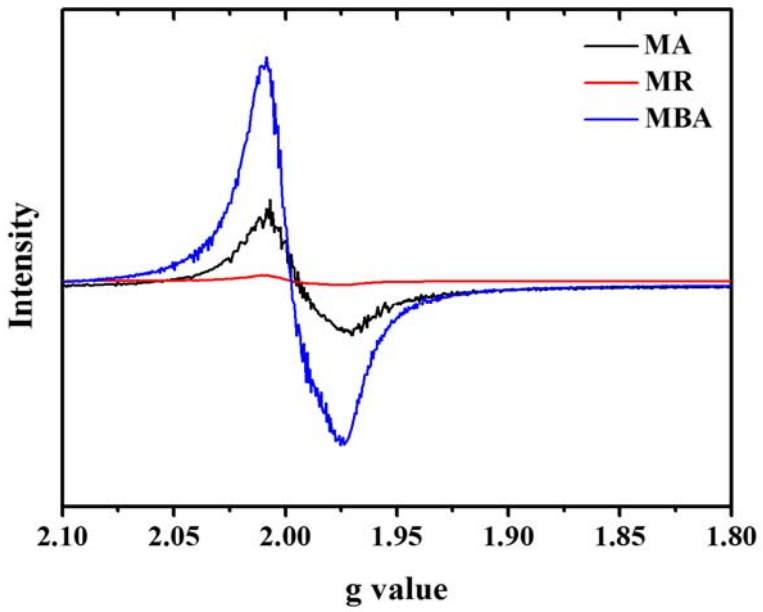

Fig. S8 Low temperature EPR spectra of MA, MR, and MBA without CN coating.

Table S1. Physical and photocatalytic properties of MBA, MBACN-*x*, CN, MACN-2, and MRCN-2

Sample	Crystal size[a)] (nm)	Valence band edge (eV)	Rate constant (min^{-1})
MBA	28.1	2.60	0.0002
MBACN-1	28.3	1.36	0.0033
MBACN-2	28.3	1.29	0.0041
MBACN-3	28.3	1.51	0.0035
CN	N/A	0.29	0.0008
MACN-2	12.6	0.25	0.0024
MRCN-2	48.4	0.12	0.0015

a) Crystal size was calculated from XRD peaks (**Fig. 3b** and **Fig. S3c**).